ONR Technical Report No. 2

12

MULTITHRESHOLD MEASUREMENT AND ANALYSIS OF PULSED LASER DAMAGE ON OPTICAL SURFACES

by

J. O. Porteus, J. L. Jernigan, and W. N. Faith
Physics Division, Michelson Laboratories
Naval Weapons Center, China Lake, CA 93555

Presented at the Ninth Boulder Damage Symposium, Materials for High Power Lasers
4-6 October 1977, Boulder, Colorado
(to be published in Proceedings)

December 1977

Research Sponsored by the
Office of Naval Research

under

Task Number RR0220202

ONR Technical Report No. 2

MULTITHRESHOLD MEASUREMENT AND ANALYSIS OF PULSED LASER DAMAGE ON OPTICAL SURFACES

by

J. O. Porteus, J. L. Jernigan, and W. N. Faith
Physics Division, Michelson Laboratories
Naval Weapons Center, China Lake, CA 93555

Presented at the Ninth Boulder Damage Symposium, Materials for High Power Lasers
4-6 October 1977, Boulder, Colorado
(to be published in Proceedings)

December 1977

Research Sponsored by the
Office of Naval Research

under

Task Number RR0220202

UNCLASSIFIED
SECURITY CLASSIFICATION OF THIS PAGE (When Data Entered)

(14) NWC-TR-2-ONR

REPORT DOCUMENTATION PAGE

READ DISTRIBUTIONS BEFORE COMPLETING FORM

1. REPORT NUMBER: Technical Report No. 2

2. GOVT ACCESSION NO.

3. RECIPIENT'S CATALOG NUMBER

4. TITLE (and Subtitle): (6) MULTITHRESHOLD MEASUREMENT AND ANALYSIS OF PULSED LASER DAMAGE ON OPTICAL SURFACES

5. TYPE OF REPORT & PERIOD COVERED: (9) Technical Report

6. PERFORMING ORG. REPORT NUMBER

7. AUTHOR(s): (10) J. O. Porteus, J. L. Jernigan, W. N. Faith

8. CONTRACT OR GRANT NUMBER(s): (16) RR022202

9. PERFORMING ORGANIZATION NAME AND ADDRESS
Naval Weapons Center
China Lake, CA 93555

10. PROGRAM ELEMENT, PROJECT, TASK AREA & WORK UNIT NUMBERS: (17) Task No. RR022202

11. CONTROLLING OFFICE NAME AND ADDRESS
Office of Naval Research (Code 471)
Metallurgy Branch
Arlington, VA 22217

(11) REPORT DATE: Dec 77

13. NUMBER OF PAGES: ~~10~~ (15) 74 pp.

14. MONITORING AGENCY NAME & ADDRESS (if different from Controlling Office)

15. SECURITY CLASS. (of this report): UNCLASSIFIED

15a. DECLASSIFICATION/DOWNGRADING SCHEDULE

16. DISTRIBUTION STATEMENT (of this Report)

Approved for public release; distribution unlimited

17. DISTRIBUTION STATEMENT (of the abstract entered in Block 20, if different from Report)

18. SUPPLEMENTARY NOTES

To be published in Proceedings of the Ninth Boulder Damage Symposium, Materials for High Power Lasers, 4-6 October 1977, Boulder, Colorado

19. KEY WORDS (Continue on reverse side if necessary and identify by block number)

Damage thresholds	Optical coatings	Surface characterization
Failure modes	Pitting	Surface uniformity
Laser-optical components	Ripples	Threshold estimation
Mo mirrors	Standard sample Au mirrors	Windows

20. ABSTRACT (Continue on reverse side if necessary and identify by block number)

See back of form.

403 019

DD FORM 1 JAN 73 1473 EDITION OF 1 NOV 65 IS OBSOLETE
S/N 0102-014-6601

UNCLASSIFIED
SECURITY CLASSIFICATION OF THIS PAGE (When Data Entered)

The methodology of multithreshold analysis, a new approach to laser-damage research, is described. The comparison of thresholds for various damage-related effects identifies dominant failure mechanisms and provides better guidance for laser-materials technology. After a brief description of apparatus, the procedure for routinely measuring up to eight different thresholds per sample is given. The maximum-likelihood principle is used to derive an algorithm for computing thresholds and standard deviations. The use of a standard gold sample to verify reproducibility and to maintain long-term calibration is discussed. Examples of multithreshold results on uncoated and coated infrared optical components are presented. The following are some of the effects for which thresholds are compared: slip, roughening, cracking, pits, melting, craters, delamination of coatings, ion and light emission, and work function change.

MULTITHRESHOLD MEASUREMENT AND ANALYSIS OF PULSED LASER DAMAGE ON OPTICAL SURFACES

J. O. Porteus, J. L. Jernigan, and W. N. Faith
Physics Division, Michelson Laboratories
Naval Weapons Center, China Lake, California 93555

The methodology of multithreshold analysis, a new approach to laser-damage research, is described. The comparison of thresholds for various damage-related effects identifies dominant failure mechanisms and provides better guidance for laser-materials technology. After a brief description of apparatus, the procedure for routinely measuring up to eight different thresholds per sample is given. The maximum-likelihood principle is used to derive an algorithm for computing thresholds and standard deviations. The use of a standard gold sample to verify reproducibility and to maintain long-term calibration is discussed. Examples of multithreshold results on uncoated and coated infrared optical components are presented. The following are some of the effects for which thresholds are compared: slip, roughening, cracking, pits, melting, craters, delamination of coatings, ion and light emission. and work function change.

Key words: Damage thresholds; failure modes; laser-optical components; Mo mirrors; optical coatings; pitting; ripples; standard sample Au mirrors; surface characterization; surface uniformity; threshold estimation; windows.

1. Introduction

The damage resistance of optics for lasers may be improved with an understanding of important damage mechanisms and their relationship to material characteristics. The comparison of thresholds for the various observable damage-related effects provides a good basis for this understanding. Some of the effects typical of a bare metal mirror may be seen in figure 1. Slip bands and intergranular slip indicate susceptibility to stress damage, which can be related to yield strength, as shown in a companion paper [1][1]. Melting, which produces the dark area in the dark-field micrograph, is an indicator of optical absorption. Laser-induced pitting, which occurs mainly on grain boundaries in figure 1, can be caused by segregated impurities. Cratering, identified by a raised rim around the melt zone, is usually caused by pressure associated with vaporization. Other effects measured by other techniques may also be informative. A change in surface work function, for example, can signal changes in surface composition or topography. Ion and light emission indicates plasma formation.

The present work presents the methodology of obtaining thresholds routinely and accurately for as many as eight different laser-induced surface effects. After a brief description of the apparatus, details of which are given elsewhere [2], the procedure for acquiring and reducing the data is discussed. The derivation of an algorithm based on the maximum-likelihood principle, which is used to compute thresholds and standard deviations, is also given. We then discuss the use of a standard gold sample to verify reproducibility and to maintain calibration. Finally, we present typical results and their interpretation on various infrared optical components.

2. Apparatus

Measurements are made in a previously described laser damage facility [2], where comprehensive target monitoring and careful beam characterization are key features. Our ultrahigh vacuum (UHV) test chamber was equipped with the following monitoring apparatus for the results presented here: (1) 20-power microscope; (2) Faraday cup with grounded entrance grid (10-mA/sr detection sensitivity at 35° off the laser beam axis) for sensing of target-emitted ions and neutrals having sufficient energy to produce secondary electrons; (3) an Auger analyzer with electron imager [2]. The electron images are generated by work function variations $\gtrsim 0.1$ eV over the target surface caused by variations in surface composition and topography.

Figure 2 illustrates the Gaussian spatial intensity distribution of the 10.6 μm laser beam when focussed on the target by a ZnSe lens having a focal length of 24 cm. Temporally, each pulse consists of a train of mode-locked spikes which form an envelope of 100 nsec nominal duration. Thresholds given are peak thresholds, i.e., they refer to the time-integrated fluence of the damaging pulse at the point of maximum spatial intensity.

---

* Work supported by the Naval Air Systems Command, the Office of Naval Research and NWC Independent Research Funds.

1. Figures in brackets indicate the literature references at the end of this paper.

The data reduction equipment consists of a Hewlett-Packard Model 9821 calculator interfaced with a Tektronix Model 4662 interactive digital plotter. Data reduction is performed entirely in the calculator, while the plotter is used only for display of final results.

3. Experimental Procedure

The sample is exposed to one pulse at each of approximately 50 sites spaced at 1-mm intervals along its surface. Pulse energies, which are measured for each pulse [2], are uniformly distributed over a range which includes the thresholds for each of the damage effects of interest. The occurrence of light emission (flash) and pit formation are noted by an observer as they occur, while damage features which are more difficult to identify, e.g., slip, melting and cratering, are categorized with the aid of more sophisticated optical microscopy after the sample has been removed from the test chamber (fig. 1). The damage observed at each site is summarized by a set of code numbers, each number representing a specific effect. The data is reduced by entering the damage summary and corresponding peak energy fluence for each site into the calculator and applying the algorithm derived below.

3.1 Threshold Algorithm

The routine determination of up to eight thresholds per sample tested requires an algorithm permitting rapid data reduction. On the other hand, effective use of available data is important, since the fluence range of thresholds is often wide, and therefore incompatible with a high density of data points. In this section we develop an algorithm which yields reproducible results with a minimum of computational complexity.

Consider the probability P_i of obtaining a certain type of damage X_i times out of N_i shots on fresh sites (1-on-1 damage) [3,4], all at the same fluence ϕ_i. This is represented by the binomial distribution

$$P_i(X_i;N_i;p_i) = \binom{N_i}{X_i} p_i^{X_i}(1 - p_i)^{N_i - X_i} \quad , \tag{1}$$

where

$$p_i = p_i(\phi_i,\phi,\sigma) \quad , \tag{2}$$

the probability of single-shot damage is a function of the damage threshold ϕ and its standard deviation σ, in addition to the fluence ϕ_i. The problem is to obtain statistical estimators for ϕ and σ in terms of the damage data X_i, N_i and ϕ_i. Our solution is based on the method of maximum-likelihood [5]. Maximizing the logarithm of the likelihood with respect to the parameters $\varepsilon = \phi$ or σ, leads to two expressions of the form

$$\sum_i \frac{\partial p_i}{\partial \varepsilon}\left[\frac{X_i - N_i p_i}{p_i(1 - p_i)}\right] = 0 \quad . \tag{3}$$

Solving simultaneously for ϕ and σ yields the corresponding maximum likelihood estimators $\hat{\phi}$ and $\hat{\sigma}$. However, the functional form of p_i is required. For computational simplicity we assume that p_i is uniformly distributed, i.e.,

$$p_i = \begin{cases} 0 & ; \ u_i \le -\frac{1}{2} \\ u_i + \frac{1}{2} & ; \ |u_i| < \frac{1}{2} \\ 1 & ; \ u_i \ge \frac{1}{2} \end{cases} \quad , \tag{4}$$

where

$$u_i \equiv \frac{\phi_i - \phi}{2\sqrt{3}\,\sigma} \quad . \tag{5}$$

Substituting eq. (4) in eq. (3), one finds that only those terms j for which $|u_j| < 1/2$ are non-zero. To further simplify the computation we neglect u_i^2 terms in the denominators, which are of the form $1/4 - u_i^2$. As a result, our estimators differ from the true maximum-likelihood estimators in that data points near $u_i = 1/2$ are less heavily weighted relative to those near $u_i = 0$. This compensates to some degree for the fact that the distribution given by eq. (4) generally represents the sample distribution less accurately near $u_i = 1/2$. Introducing eq. 5) and solving for ϕ yields

$$\hat{\phi} \simeq \frac{[\sum \phi_j^2 N_j][\sum (X_j - \frac{1}{2}N_j)] - [\sum \phi_j N_j][\sum \phi_j (X_j - \frac{1}{2}N_j)]}{[\sum \phi_j N_j][\sum (X_j - \frac{1}{2}N_j)] - [\sum N_j][\sum \phi_j (X_j - \frac{1}{2}N_j)]} \quad . \tag{6}$$

Solving for σ gives

$$\hat{\sigma} \simeq \frac{1}{2\sqrt{3}} \frac{\sum \phi_j N_j - \hat{\phi} \sum N_j}{\sum (X_j - \frac{1}{2}N_j)} \quad ; \quad \sum (X_j - \frac{1}{2}N_j) \neq 0 \quad , \tag{7a}$$

but gives the indeterminate form 0/0 when $\sum (X_j - \frac{1}{2}N_j) = 0$. Noting that eq. (6) defines the sample mean of ϕ_j under the latter condition, we infer that

$$\hat{\sigma} \simeq \sqrt{\frac{\sum \phi_j^2 N_j}{\sum N_j} - \left(\frac{\sum \phi_j N_j}{\sum N_j}\right)^2} \quad ; \quad \sum (X_j - \frac{1}{2}N_j) = 0 \quad . \tag{7b}$$

It follows from the definition of j that eqs. (6) and (7) apply only to data within the interval

$$\left| \frac{\phi_j - \phi}{2\sqrt{3}\,\sigma} \right| < \frac{1}{2} \quad . \tag{8}$$

While the estimators $\hat{\phi}$ and $\hat{\sigma}$ are expressed entirely in terms of the damage data, the data interval given by eq. (8) involves the unknowns ϕ and σ, and must be determined by trial and error. A satisfactory method for this has been developed, and is included in the routine data reduction procedure described below.

3.2 Data Reduction

Equations (6) through (8) are applied to each damage effect in turn via the calculator as follows. Fluences associated with the code number corresponding to a particular effect are sorted into a damaging, and the remaining fluences into a nondamaging category. Damaging fluences are then arranged and listed in order of ascending value, while the nondamaging fluences are listed in descending order. Data near the head of each list is examined for consistency by the operator and reclassified or discarded as required. Equations (6) and (7) are then applied to the revised lists. The j summations are initially taken over all data in the smallest interval which (a) includes the lowest damaging and highest nondamaging fluence, and (b) includes a damaging and nondamaging fluence as upper and lower limits, respectively. The interval is then extended as required to provide the minimum value of $\hat{\sigma}$, determined by applying eq. (7) to each new interval. This minimum $\hat{\sigma}$ and the $\hat{\phi}$ obtained by applying eq. (6) to the same interval are taken as the final results for the effect in question. In practice, it is found that $\hat{\phi}$ is rather insensitive to the data interval. However, $\hat{\sigma}$ depends more strongly on the number of data points used and their separation. Given adequate data the major contribution to $\hat{\sigma}$ usually comes from the variation of the damage threshold across the sample surface, with a relatively small contribution coming from the experimental uncertainty.

Repeated application of the algorithm gives an average threshold, together with its standard deviation, for each effect. The resulting thresholds for the target are presented in the form of a bar graph or damage profile, examples of which are presented below.

3.3 Reproducibility and Long-Term Calibration

The reproducibility of the threshold results can be demonstrated by repeated application to a sample with uniform damage characteristics over its surface, as indicated by relatively small standard deviations of the damage thresholds. A mirror produced by electrodeposition of Au on diamond-turned bulk Cu has this desirable property. The oxidation resistance is an added advantage, which makes this sample especially attractive as a standard for calibration maintenance. The ability to directly standardize damage thresholds is an invaluable asset in the long-term development of damage-resistant optical components.

Figure 3 presents the results of two independent multithreshold measurements on the standard gold sample. Figure 3(a) was obtained before, and figure 3(b) after replacing the output coupler on the laser over one month later. After correction for a 10% change in focal spot diameter, the thresholds for all effects listed except one agree within the combined standard deviations given. Statistically, approximately half the thresholds should agree this well when the effects are independent. It is clear that changing the output coupler had negligible effect on the calibration. Furthermore, we may conclude that the threshold algorithm gives consistent and reproducible results, the accuracy of which is conservatively represented by the standard deviations.

3.4 Examples

Multithreshold analysis has been applied to a variety of infrared mirror and window surfaces prepared by various techniques. Both coated and uncoated samples have been studied. The present section gives a few representative examples of results obtained.

The application of multithreshold analysis to relate damage mechanisms to surface characteristics of bare metal mirrors, particularly Cu, has been amply demonstrated [1]. Certain aspects of the Au mirror represented in figure 3 were also discussed. To complete this discussion it should be pointed out that the relatively high slip threshold indicated in figure 3 may be influenced by the difficulty in observing slip on this sample [1]. In fact, the lowest threshold is for work-function change, which is attributed to evolution of water by the Au layer. This result is supported by a laser-induced diminution of oxygen as observed by Auger.

The value of multithreshold analysis in evaluating nominally equivalent mirror finishes is illustrated in figure 4, where we compare damage profiles of Mo mirrors polished by two different vendors. While mirror A exhibits higher thresholds for most types of damage, including melting, it is far more susceptible to pitting and associated plasma formation. The superior uniformity of mirror B is also evident in the smaller standard deviations.

As an example of multithreshold results from a window material we compare profiles for damage occurring on the entrance (front) and exit (back) surfaces of a polished NaCl blank (fig. 5). Only those sites where no simultaneous damage was observed on the front surface are represented in figure 5(b). All thresholds on the front are essentially the same, indicating breakdown as the only damage mechanism. Thresholds at the back surface are generally lower because of the constructive phase relationship between incident and reflected fields. Effects peculiar to the back surface are ripples, pits and fracture. Ripples result from the interference of incident and scattered radiation [6]. Present evidence shows that ripples occur only in the presence of a plasma. The pits may represent scattering sources for the ripples. The fact that pits occur only on the back surface suggest that they result from bulk, rather than from surface inhomogeneities. Scrubbing associated with the plasma, which was observed in mirrors [1], has also been observed on this sample.

A damage profile from an enhanced-reflection coating on polished bulk Cu is shown in figure 6. The thresholds are well below those for bare Cu. Pitting due to coating defects is the dominant failure mode. Almost identical damage profiles were obtained when the same coating design was applied to Mo and to ULE glass.

Figure 7 compares damage thresholds from As_2S_3 in bulk form, and as a coating [7] on the NaCl. In the bulk material the coincidence of thresholds for surface pitting and bulk damage suggest that these result from the same mechanism which, surprisingly, is active below the threshold for pitting in the coating. Also, pitting in the coating tends to associate with a plasma, which is not true in the bulk material.

4. Summary

An efficient and reliable method has been developed for simultaneously measuring the thresholds and standard deviations for up to eight laser-damage-related effects on a single sample. An algorithm based on the maximum-likelihood principle has been derived for computing results directly from the experimental data. Reproducibility has been demonstrated by repeated measurements on a standard Au sample. The use of this sample to maintain long-term calibration was described. Examples of multithreshold results on representative optical components of each type have been given and the principal weaknesses of these components identified. The comparative analysis of such results from well characterized samples prepared from different materials and by different techniques yields the relationship between damage thresholds and material characteristics. These comparisons can also provide a better understanding of laser-damage mechanisms.

5. Acknowledgments

The authors are indebted to G. J. Sorenson for programming the plot routine for the damage profiles.

6. References

[1] Porteus, J. O., Fountain, C. W., Jernigan, J. L., Faith, W. N. and Bennett, H. E., this conference.

[2] Porteus, J. O., Soileau, M. J. and Bennett, H. E., in *Laser Induced Damage in Optical Materials: 1975*, A. J. Glass and A. H. Guenther, eds. (NBS Spec. Publ. 435), p. 207.

[3] Bass, M. and Leung, K. M., IEEE J. Quantum Electron. QE-12, 32 (1976).

[4] For n-on-1 damage the situation is obviously equivalent if nondamaging pulses leave an equivalent damage probability at each site.

[5] Mood, A. M., *Introduction to the Theory of Statistics* (McGraw-Hill, New York, 1950), Ch. 8.

[6] Temple, P. A. and Soileau, M. J., in *Laser Induced Damage in Optical Materials: 1976*, A. J. Glass and A. H. Guenther, eds. (NBS Spec. Publ. 462), p. 371.

[7] Donovan, T. M., Baer, A. D., Dancy, J. H. and Porteus, J. O., this conference.

7. Figures

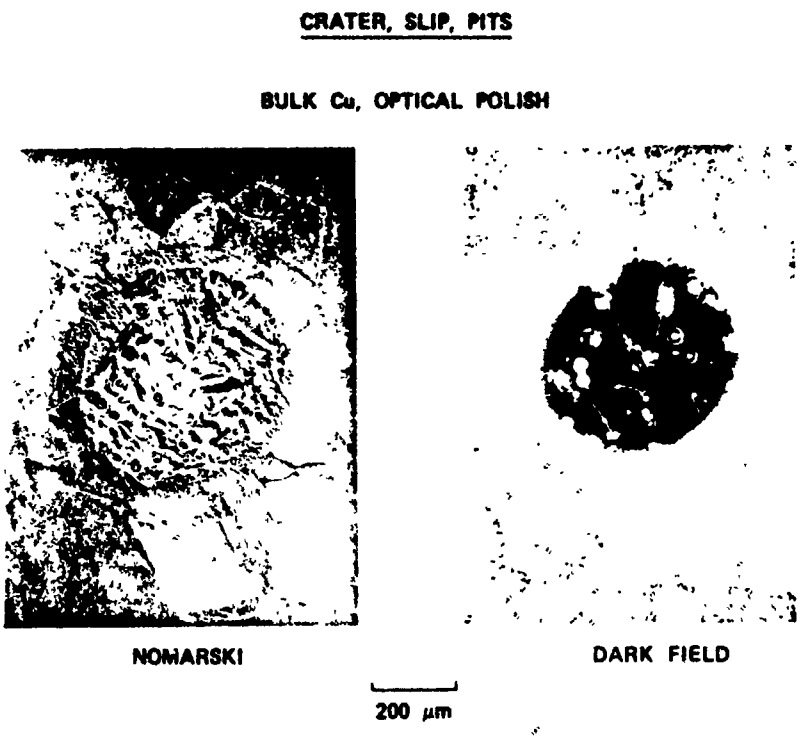

Figure 1. Micrographs of visible damage on polished bulk Cu at a peak fluence of 68.3 J/cm^2. In Nomarski, slip bands appear outside the crater at the 5 o'clock position, while intergranular slip is responsible for prominent crack-like features.

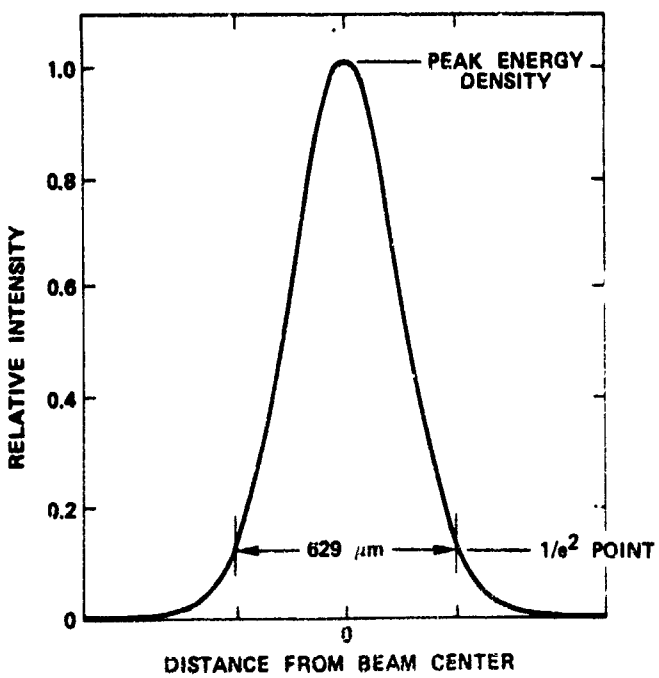

Figure 2. Gaussian spatial profile of focussed laser pulse, showing $1/e^2$ width and peak energy density (fluence) at which thresholds are determined.

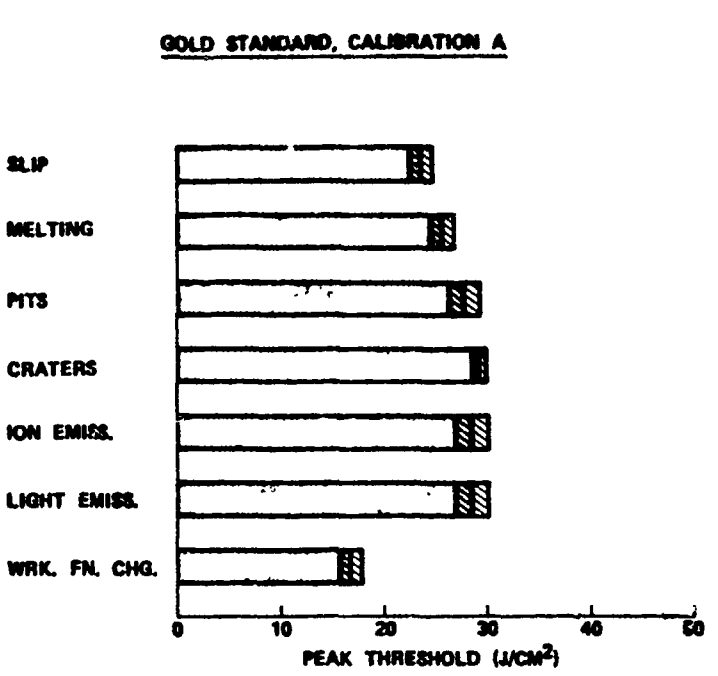

Figure 3(a). Damage profile of standard gold sample, measured for calibration with the original laser output coupler. Thresholds are indicated by the shaded bars. Standard deviations (+ or -) are indicated by the semishaded boxes at the ends of the bars.

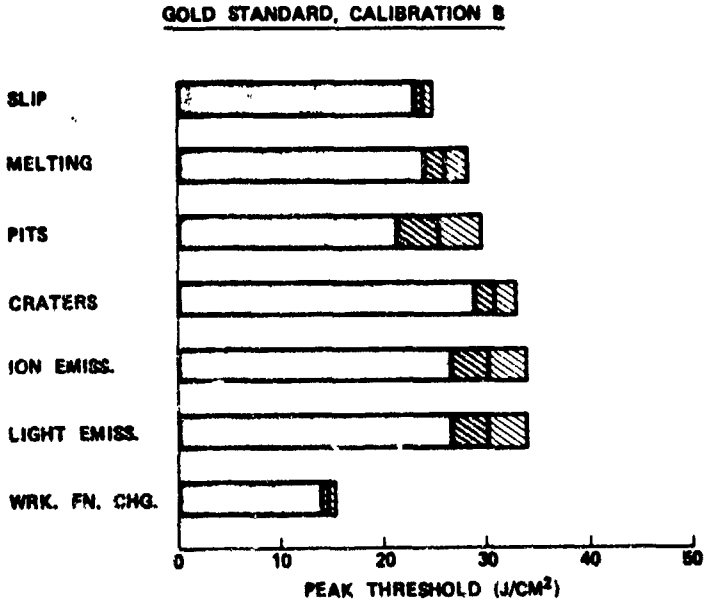

Figure 3(b). Damage profile to be compared with figure 3(a), measured for calibration with new laser output coupler.

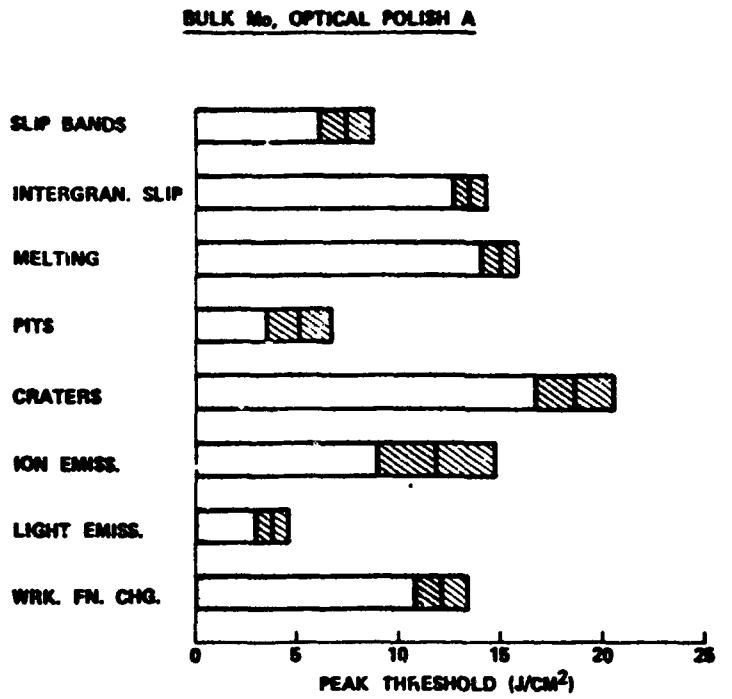

Figure 4(a). Damage profile of polished bulk Mo from vendor A.

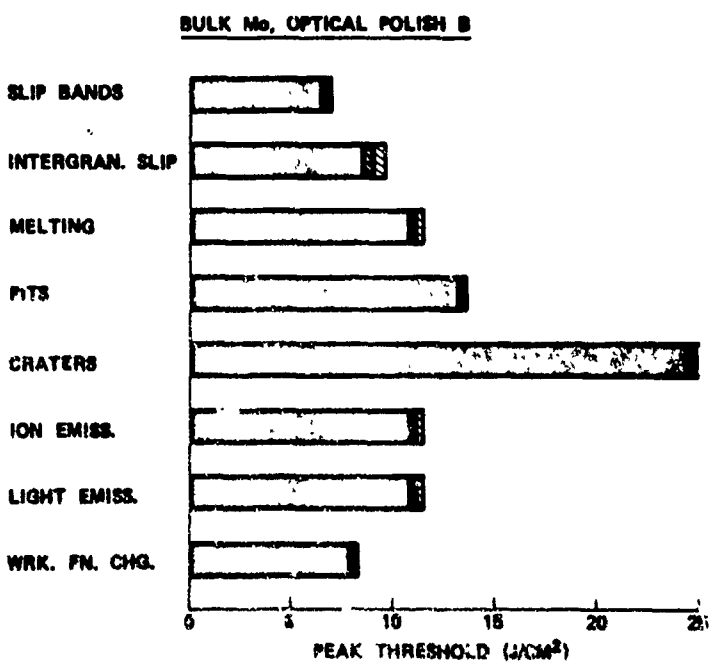

Figure 4(b). Damage profile of polished bulk Mo from vendor B.

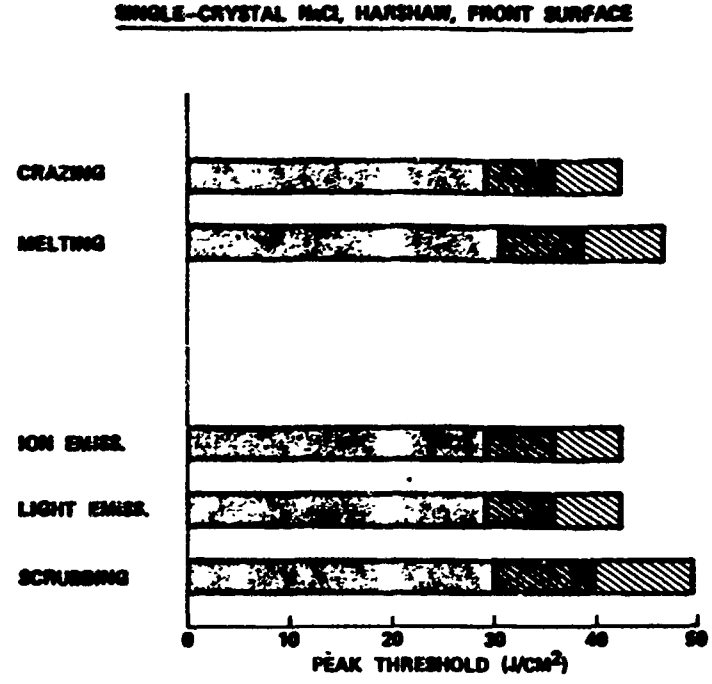

Figure 5(a). Front surface damage profile of a NaCl blank, 6.4-mm thick, polished on both surfaces.

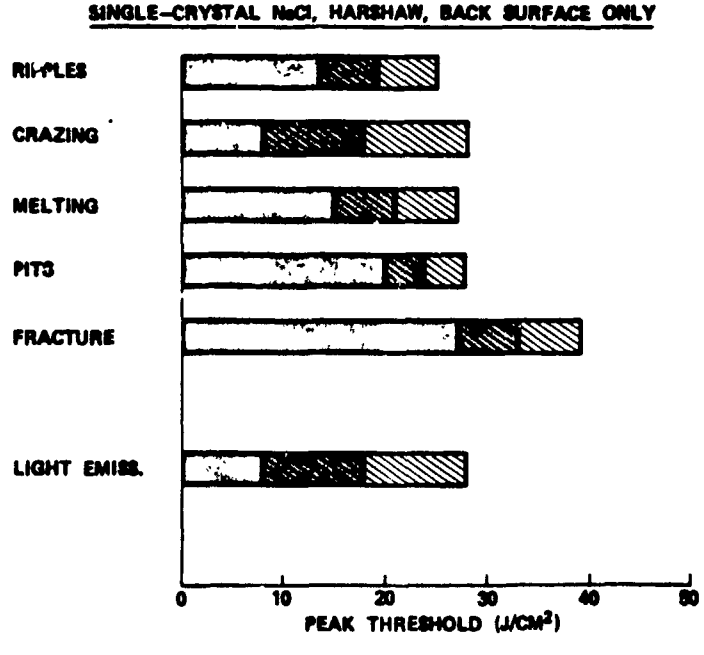

Figure 5(b). Profile of damage occurring only on the back surface of the same blank. The laser beam was focussed on the front surface.

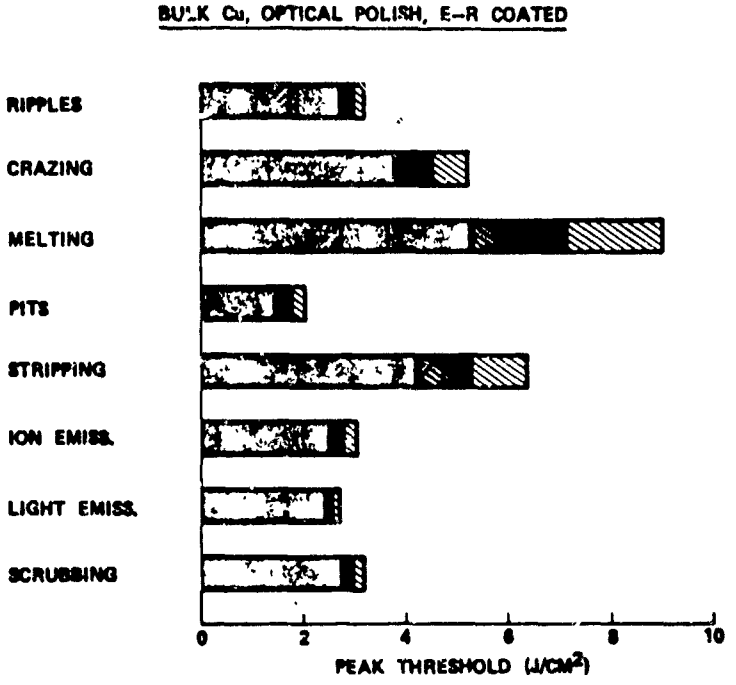

Figure 6. Damage profile of a 10.6-μm enhanced reflection coating on bulk Cu. Coating consists of alternating layers of Ge and ZnS on a thin Ag layer.

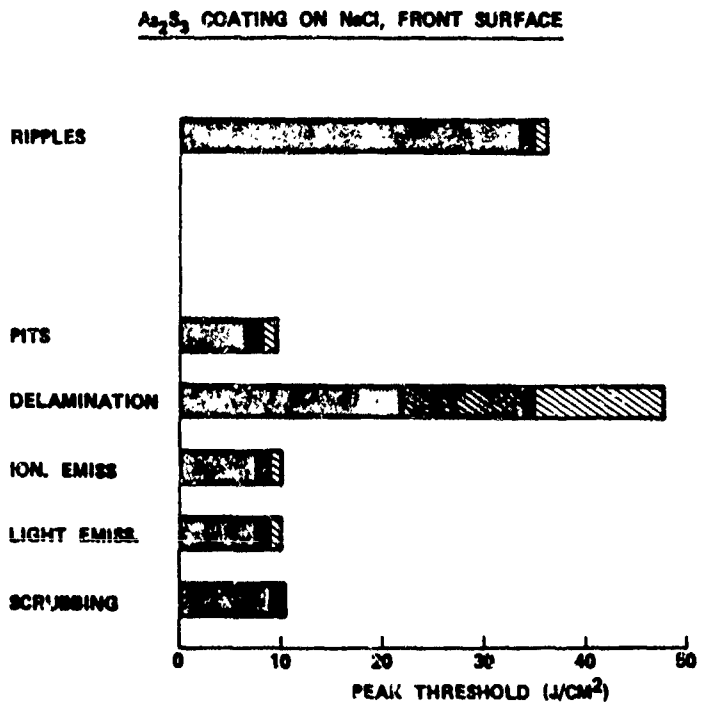

Figure 7(a). Damage profile of an As_2S_3 coating on the front surface of NaCl.

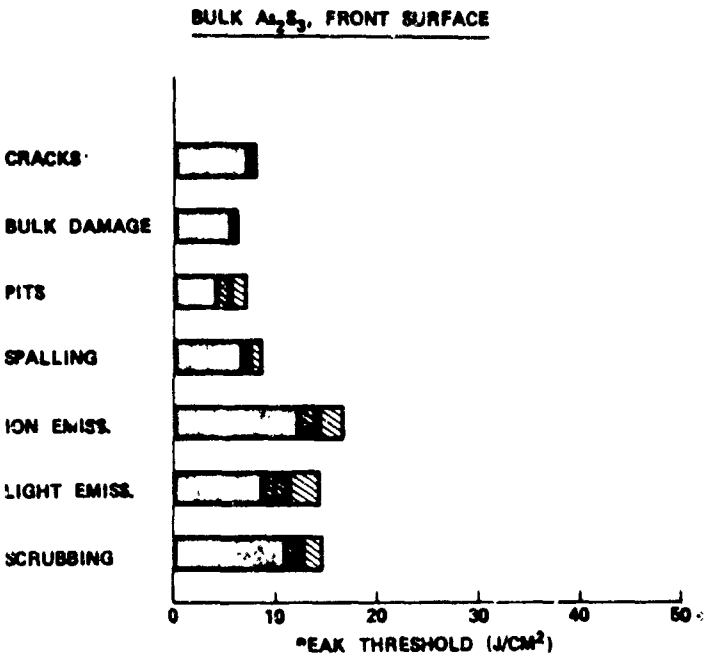

Figure 7(b). Damage profile of polished bulk As_2S_3.